Turkish Journal of Electrical Engineering & Computer Sciences

http://journals.tubitak.gov.tr/elektrik/

Research Article

Turk J Elec Eng & Comp Sci
(2017) 25: 3501 – 3514

doi:10.3906/elk-1605-2

A linear magnetorheological brake with multipole outer coil structure for high on-state and low off-state force outputs

Özgür BAŞER[1,*], Mehmet Alper DEMİRAY[1], Aytuğ BAŞ[1], Ergin KILIÇ[1], Galip Ozan EROL[2]

[1]Department of Mechanical Engineering, Faculty of Engineering, Süleyman Demirel University, Isparta, Turkey
[2]Department of Mechanical Engineering, Faculty of Engineering, University of Delaware, Newark, DE, USA

Received: 03.05.2016 • **Accepted/Published Online:** 01.11.2016 • **Final Version:** 05.10.2017

Abstract: A wide range of braking forces, from near zero to high values, is required in specific applications such as forces in haptic devices or steering stability in motorcycles. Classical piston cylinder type magnetorheological (MR) brakes are not suitable for these applications due to their high off-state forces. In this paper, a new linear type MR brake employing shear mode braking principle with a multipole outer coil structure is presented for high on-state and low off-state force outputs. To implement this device, an analytical model of the brake is derived by using magnetic circuit analysis to determine braking force. Magnetic finite element models are developed and coupled with an optimization algorithm to determine the optimal set of parameters of the brake design. A prototype is manufactured and tested experimentally to characterize the device's force response, transient response, hysteresis, force tracking, and damping performance. The proposed brake achieved a maximum braking force of 480 N and a low off-state force of 6 N with infinite stroke. The results show that the ratio of maximum force to off-state force for our device is about 80, even though it is a maximum of 32 for the best linear brakes in the literature.

Key words: Linear magnetorheological brake, multipole coil, braking force

1. Introduction

Magnetorheological (MR) brakes provide variable braking force for many applications, such as automotive steering stability, brake systems, haptics, and stability in robotics. A wide range of force profiles (from near zero to high forces) is required for robotic applications. In particular, it is a must for the haptic applications for the transparency and stability. Some of the haptic applications that employ MR brakes for passive device forces/torques were presented in [1–4]. In the literature, there are various classical piston cylinder MR brakes. Lord Corporation has produced commercial MR brakes for many applications; for example, Model RD-1005, produced by Lord Corporation, has a diameter of 38 mm and stroke length of 208.3 mm, and its maximum force is 451 N at 0.2 m/s with 1.5 A current input. However, it has an off-state force of about 52 N when no magnetic field is applied [5–7]. This means that this brake has a maximum force to off-state friction force ratio of 8.7. Another commercial product by Lord Corporation, Model SD 1000-2, has diameter of 44.45 mm and nominal stroke length of 101.6 mm [8]. This brake can produce 2.1 kN maximum force output at 1.5 A of current at a velocity of 0.2 m/s. Nonetheless, the off-state force is approximately 270 N. Its ratio of maximum force to off-state friction force is about 7.8. Another linear MR brake, with a size of 130 mm in length and

*Correspondence: ozgrbasr@gmail.com

30 mm in diameter, is used in a prosthetics application [9]. For this brake, the maximum force is 942 N and off-state friction is about 94 N. Its ratio is about 10. Another MR brake, developed in [10], produces 12 kN of maximum force with 1.5 A at 0.5 m/s velocity and 4 kN of off-state friction force. Its ratio is about 3. Another linear MR brake with diameter of 48 mm outputs 4 kN at 10 A and 0.3 kN when it is deactivated [11]. Its ratio is about 13.3. In addition to these designs, Shiao et al. [12] applied a multicoil structure on the piston of the conventional type linear MR brake to improve the maximum force. The original idea of the multipole coil structure was applied to rotary MR brakes by Shiao et al. [13,14], who improved the torque performance considerably. Implementing a multicoil structure on the classical piston cylinder type linear MR brake improved the maximum force up to 500 N; however, the off-state force could not be decreased, and it is approximately 65 N. The pressure difference between the piston surfaces in this design still causes high friction force and the ratio of maximum force to off-state force is about 7.7 at 0.03 m/s [12]. As can be seen from these studies, on-state maximum force outputs of conventional linear MR brakes in the literature is less than 13.3 times their off-state friction force. The classical piston cylinder type design is not an appropriate solution for robotic applications, since it cannot provide high braking forces with small off-state frictional forces. The classical piston cylinder type linear brakes use the valve mode braking principle. However, employing the shear mode principle for linear MR brakes would be more reasonable for improving force outputs while reducing the off-state friction force. In the shear mode principle, the stator of the brake is stationary and a single rod type piston inside the stator is moving. When a thin MR fluid layer between the stator and piston is activated by magnetic flux, a resistance force can be achieved due to the high shear stress on the piston surface. Only viscous and Coulomb frictions exist when the brake is off-state. In this way, the high off-state friction force resulting from the high pressure difference between the two faces of the piston in the classical MR brakes can be eliminated. However, the efficient activation of this MR fluid layer is a challenging problem.

Alkan et al. first applied the shear mode braking principle by using the serpentine flux path concept on linear MR brakes [15]. The serpentine flux path concept was first introduced by Blake and Gurocak for rotary MR brakes [16]. According to this concept, magnetic flux was weaved by nonferromagnetic and ferromagnetic plates to enlarge the activated MR fluid on the gap surface. In this way, higher braking torque was achieved in rotary MR brakes. Through the linear MR brake design, applied with the serpentine flux path concept, Alkan et al. achieved 173 N of maximum force and 5.4 N off-state friction. Its ratio of maximum force to off-state force is about 32 [15].

To improve this ratio further, we propose using a multipole coil structure on the stator of the linear MR brake. With this new solution, our design produces higher on-state force while keeping off-state friction at low levels. In this design, multipole coils multiply the magnetic flux path, which can activate the largest amount of MR fluid more efficiently. The maximum on-state and off-state force of the proposed design is 480 N and 6 N, respectively. Thus, the ratio of maximum on-state to off-state force is increased to 80.

In the remaining part of this paper, the design configuration, analytical modeling, magnetic circuit analysis, design optimization, and magnetic finite element analysis (FEA) of the multipole outer coil linear brake design are introduced. Its manufacturing details and experimental results are also included. Finally, the discussion and conclusion of the paper are presented.

2. Linear MR brake with multipole outer coil design

2.1. Design of the conventional linear MR brakes

Most linear MR brake designs that are available commercially and in the literature are designed to replace regular shock dampers. The most common design includes a piston, where the coils are attached at the outer

surface to generate a magnetic field, while MR fluid is between the outer casing and the piston of the MR brake (Figure 1). High pressure differences between the two faces of the piston along with the activated MR fluid can produce high forces. However, this design feature also leads to high off-state forces, even if the MR fluid is not activated. The drawback of the conventional design was illustrated by Alkan et al. [15]. Off-state force due to the pressure difference was calculated as 71 N for Li et al.'s design at 30 mm/s [9]. This disadvantage restricts the use of the conventional design in applications such as robotics where low off-state forces are desired.

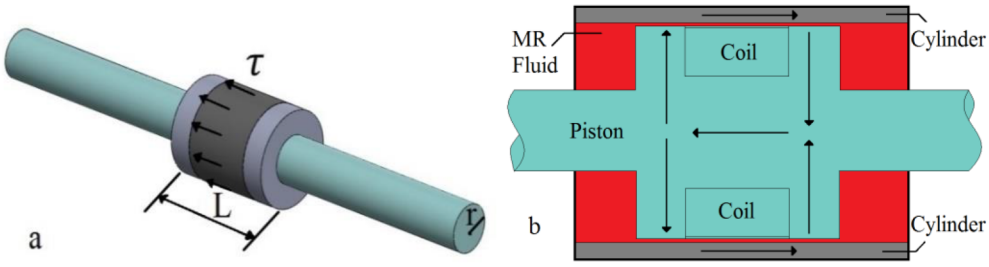

Figure 1. (a) Solid model view of the piston, (b) magnetic flux path around the section view of coils [15].

2.2. Design of the linear MR brake with multipole coil design

The conventional MR brake designs use pistons that have embedded ring type coils to activate the MR fluid. However, this design increases the area through which the magnetic flux passes, resulting in low magnetic flux density and therefore low force outputs. This problem can be solved by increasing the piston radius, the number of ring type coil windings, or the coil current. However, these solutions have drawbacks and lead to either bulkier designs with high inertias or to overheating of the devices [17].

In this work, the proposed linear MR brake design employs multiple coils that are attached to the circular outer casing rather than to the piston in order to reduce the inertia of the piston, as shown in Figure 2a. There is a total of 6 coil windings that are symmetrically placed. Multiple coils allow the activation of MR fluid over a large area, providing high force output, as shown in Figure 2b. Moreover, the inertia of the piston is further reduced by employing a hollow piston design. MRF-140CG by Lord Corporation was selected because of its superior properties compared to other commercial MR fluids, such as high yield stress [18–20]. The properties of commercial magnetorheological fluids (MRFs) are given in Table 1. Magnetically conductive AISI 1010 steel and nonconductive aluminum parts were used in the design to form the magnetic path. The coils around the outer casing were constructed using AWG-30 copper wire.

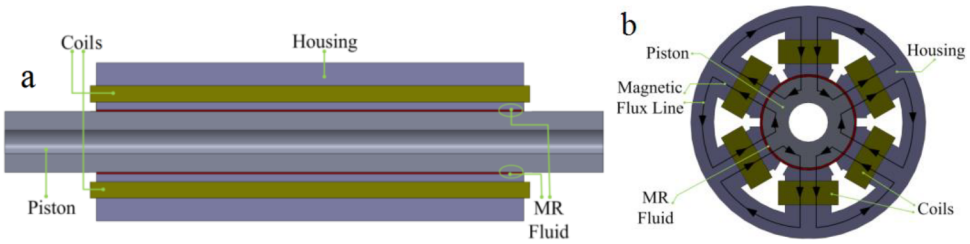

Figure 2. a) Conceptual design of the linear MR brake with multipole coil design, (b) magnetic flux path when the brake is activated.

Important design parameters of the proposed design are shown in Figure 3. These parameters were chosen because they directly affect the size of the design and the magnetic flux path, which eventually influence the design's force output.

Table 1. Properties of commercial magnetorheological fluids (MRFs) [18–20].

MRF-122CG	MRF-132DG	MRF-140CG	Property
Hydrocarbon	Hydrocarbon	Hydrocarbon	Carrier liquid
2.28	3.09	3.64	Density (g/cm^{-3})
23	23	38	Yield stress (kPa at 100 kA m^{-1})
42	112	280	Plastic viscosity (mPa s at 40 °$^{-1}$)
–40 to 130	–40 to 130	–40 to 130	Operational temperature (°)
0.21–0.81	0.25–1.06	0.28–1.28	Thermally conductive(Wm^{-1}°$^{-1}$at 25 °)
6.5 × 10^{-4}	5.5 × 10^{-4}	5.0 × 10^{-4}	Thermal expansion coefficient (0–50 °)

Parameter	Formula
Rotor-ring thickness	$t_r = R_2 - R_1$
Rotor Radius	$R_r = R_2$
Stator-ring thickness	$t_s = R_6 - R_5$
Stator Radius	$R_s = R_6$
MR-fluid gap	$g = R_3 - R_2$
Slot	s
Coil core thickness	c
Axial width	z

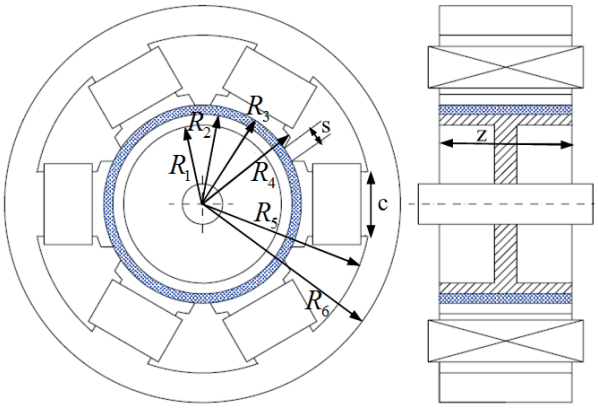

Figure 3. Design parameters of the proposed brake design [14].

MR fluid's viscous shear behavior is generally modeled with the Bingham plastic model [21,22]. The yield stress in this model is given as:

$$\tau = \tau_y + \eta\dot{\gamma}, \tag{1}$$

where τ, τ_y, η, and $\dot{\gamma}$ are total shear stress, yield stress due to magnetic flux, viscosity of the MR fluid, and shear rate, respectively. The force output can be estimated by using Eq. (1) and assuming linear fluid velocity distribution across the fluid gap and no slip condition. Hence, the shear rate in Eq. (1) can be expressed as [23]:

$$\dot{\gamma} = v/g, \tag{2}$$

where ν and g are linear velocity and MR fluid gap, respectively. The shear stress can be expressed in terms of the magnetic induction by using curve fitting on the data provided by the manufacturer's datasheet of the MR fluid. A third-order curve was fit for the MRF-140CG:

$$\tau_y = -2.8\times10^{-29}\times H^3 - 1.4\times10^{-9}\times H^2 + 0.00059 \times H + 0.84. \tag{3}$$

Infinitesimal force due to the magnetic field and frictional forces can be expressed as:

$$dF = dF_{MR} + dF_{fr}, \tag{4}$$

where dF_{MR} and dF_{fr} correspond to infinitesimal forces due to the magnetic field and frictional forces,

respectively. Integrating Eq. (4) along the piston surface gives the total force output of the brake as:

$$dF = z \int_0^{2\pi} R_r \tau_y d\theta dz + \frac{2\pi n v}{g} z + F_{fr}. \tag{5}$$

Eq. (5) involves three different force components that contribute to the total braking force of the brake: force created by the activation of the MR fluid, viscous forces, and Coulomb frictional forces. The first part of Eq. (5) is the controllable part of the total output and it can be optimized to obtain higher forces by changing the brake design. On the other hand, the other terms are not controllable and should be accounted for in the design.

2.3. Magnetic circuit analysis

A preliminary magnetic circuit analysis was carried out to determine the design parameters that might have an effect on the amount of magnetic flux generated on the MR fluid by the coils. The results of the magnetic circuit analysis are then used to obtain information about which parameters might affect the magnetic field stress. Finally, the parameters found to have significant effects on the magnetic field stress are used to optimize the brake design. In the proposed design, only one-sixth of the brake was analyzed using magnetic circuit analysis, because of symmetry. Figure 4 shows the magnetic circuit of the proposed MR brake with coil windings (magnetomotive force) and the flux path consisting of magnetically conductive and nonconductive materials.

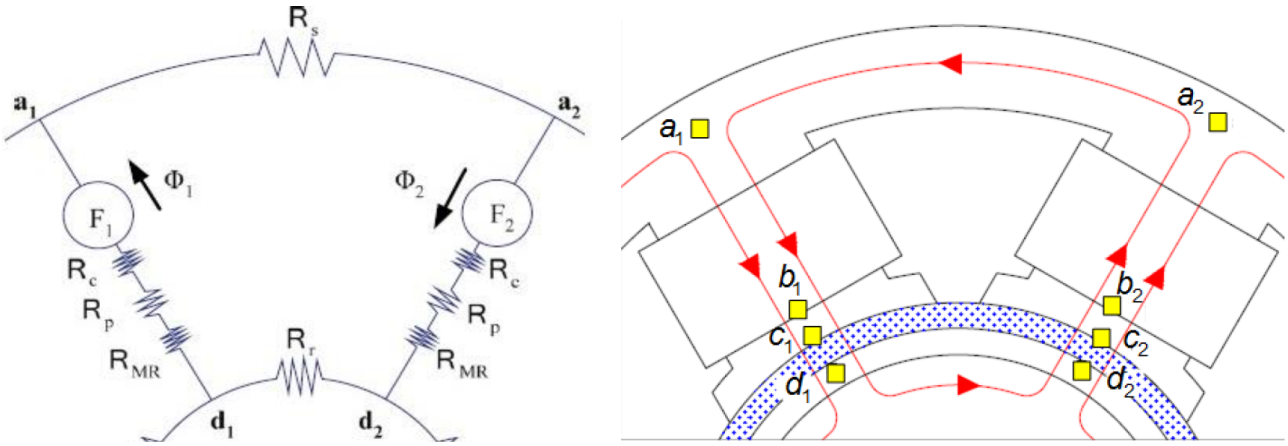

Figure 4. Magnetic circuit [14].

The path shown in Figure 4 provides resistance to the magnetic flux that is called reluctance (R). This resistance can be calculated by summing up reluctances of each individual section that is present in the flux path: MR fluid, the coil, the pole head, and steel sections. The magnetic flux generated (‘) in the path can then be calculated using the reluctance as follows:

$$\Phi = NI/R \text{ and } R = l/\mu A, \tag{6}$$

where N, I, μ, l, and A correspond to the number of coil windings, current, magnetic permeability of a specific section, length, and the cross-sectional area of the section, respectively. The magnetic flux across the MR

fluid can be estimated in terms of the permeability and dimensions of the sections. It was assumed that the cross-sectional areas of the core, namely the MR brake and the pole-head sections, are the same. Furthermore, the magnetic permeability of the steel sections was assumed as in [14]:

$$1000\mu_{MR} \approx \mu_{steel}. \tag{7}$$

Then the magnetic flux on the MR fluid can be expressed as:

$$H_{MR} = 4NI/(4g + c(\mu_{MR}/\mu_s)(R_s/t_s - R_r/t_r)). \tag{8}$$

Eq. (8) provides an important relationship showing how the design parameters affect the magnetic flux strength of MR fluid of the brake. FEA can be employed to compute an accurate force generated by the MR fluid. Yield stress formulation as a function of magnetic field strength, the first term in Eq. (5), can be employed in a functional FEA program such as ANSYS Maxwell and more precise optimization can be achieved.

2.4. Finite analysis and optimization of the design

Optimal parameters of the proposed design were determined using magnetic FEA and the sequential nonlinear programming optimization technique. A parametric model of the design was created in ANSYS Maxwell to carry out the magnetic FEA simulations and determine the optimal design parameters.

Rotor, stator, stator core thicknesses, and slot dimensions were chosen as the design optimization parameters, while magnetomotive force, rotor and stator radius, rotor width, and MR fluid gap were chosen as the fixed design parameters. The fixed design parameters were chosen to obtain a specific actuator volume for the intended application. Table 2 shows the values selected for the fixed design parameters along with the ranges used for the design optimization parameters.

Table 2. Design parameter values.

Fixed design parameters		Design parameters for optimization			
Parameter	Value	Parameter*	Range	Optimal value	Prototype value
Magnetomotive force	100$^+$	Rotor thickness t_r	2–6	5.89	6
Rotor radius R_r	10	Stator thickness t_s	2–6	5.20	5
Stator radius R_s	25	Stator core thickness c	7–10	9.86	10
Rotor/stator width z	110	Slot s	2–5	2.02	2
MR fluid gap g	0.5				

*Dimensions are in mm. $^+$Unit: Ampere-turn.

The materials selected from Maxwell material library were ANSI 1010 steel for the stator and rotor and copper for the coil wire. The magnetization of ANSI 1010 steel is given in Table 3. The Maxwell material library does not include a material model for MR fluid. Therefore, MR fluid material properties for MRF-140CG were implemented as a new material. The range of the core thickness was determined to avoid magnetic saturation while obtaining sufficient space for the coils. Rotor and stator thickness ranges were determined based on the manufacturing capabilities. Moreover, the slot thickness range was chosen based on the overall size and individual coil size. The design criterion was chosen as the maximum magnetic field force, and a cost function was defined by maximizing the first term of Eq. (5), as given below:

$$F_{field} = \int_0^z \int_0^{2\pi} R_r \tau_y d\theta dz. \tag{9}$$

Table 3. Magnetization of ANSI 1010 steel.

H (A/m)	B (T)
0	0
238.7	0.2003
318310	0.3204
358.1	0.40045
437.7	0.50055
477.5	0.5606
636.6	0.7908
795.8	0.931
1114.1	1.1014
1273.2	1.2016
1591.5	1.302
2228.2	1.4028
3183.1	1.524
4774.6	1.626
6366.2	1.698
7957.7	1.73
15,915.5	1.87
31,831	1.99
47,746.5	2.04
63,662	2.07
79,577.5	2.095
159,155	2.2
318,310	2.4

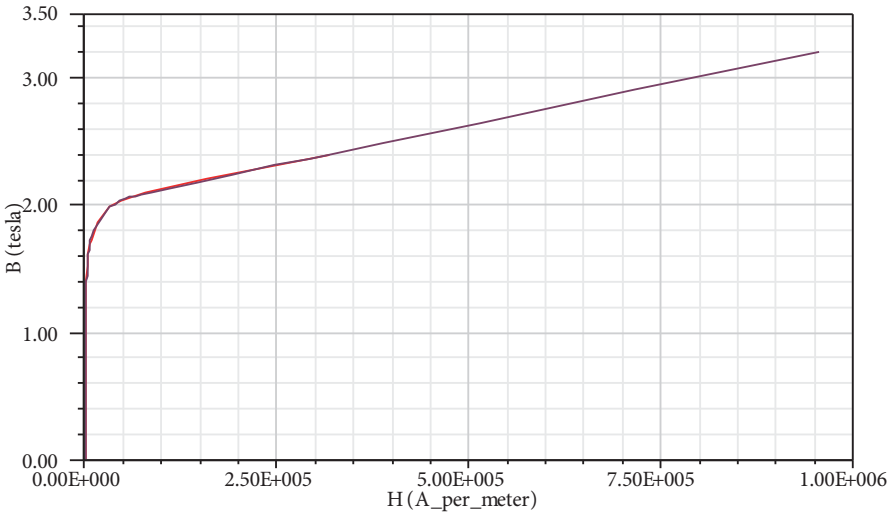

The maximum number of iterations for the optimization was set to 100. The 38th iteration gives the maximum field force. The optimal design parameter values are presented in Table 2. Figure 5 shows the magnetic field created across the MR fluid gap at different current levels. Note that this figure shows the results at optimal design parameters.

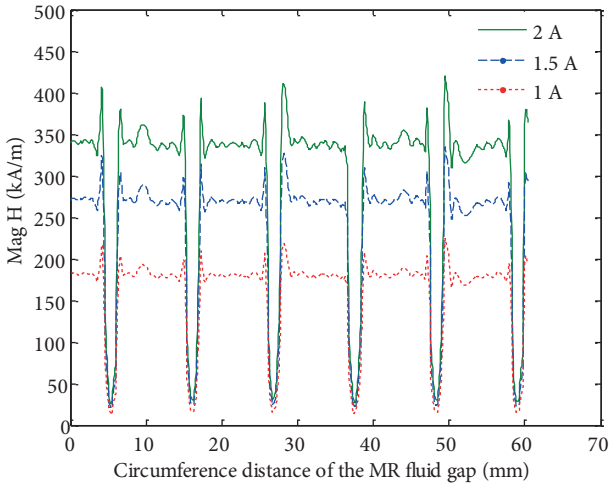

Figure 5. Magnetic field at different input currents.

Figure 6a shows the distribution of the magnetic field at 1 A in the optimized design. Figure 6b shows the magnetic flux in vector form. The magnetic induction generated across the MR fluid is presented in Figure

6c. This figure shows that the rotor and stator are not saturated at 1 A, since the maximum induction is approximately 1.5 T, which is much lower than the saturation level of 2.3 T of ANSI 1010 steel. It can be seen in Figure 6d that the magnetic induction is almost uniform across the MR fluid except for the slot regions, where the magnetic induction is low compared to other regions.

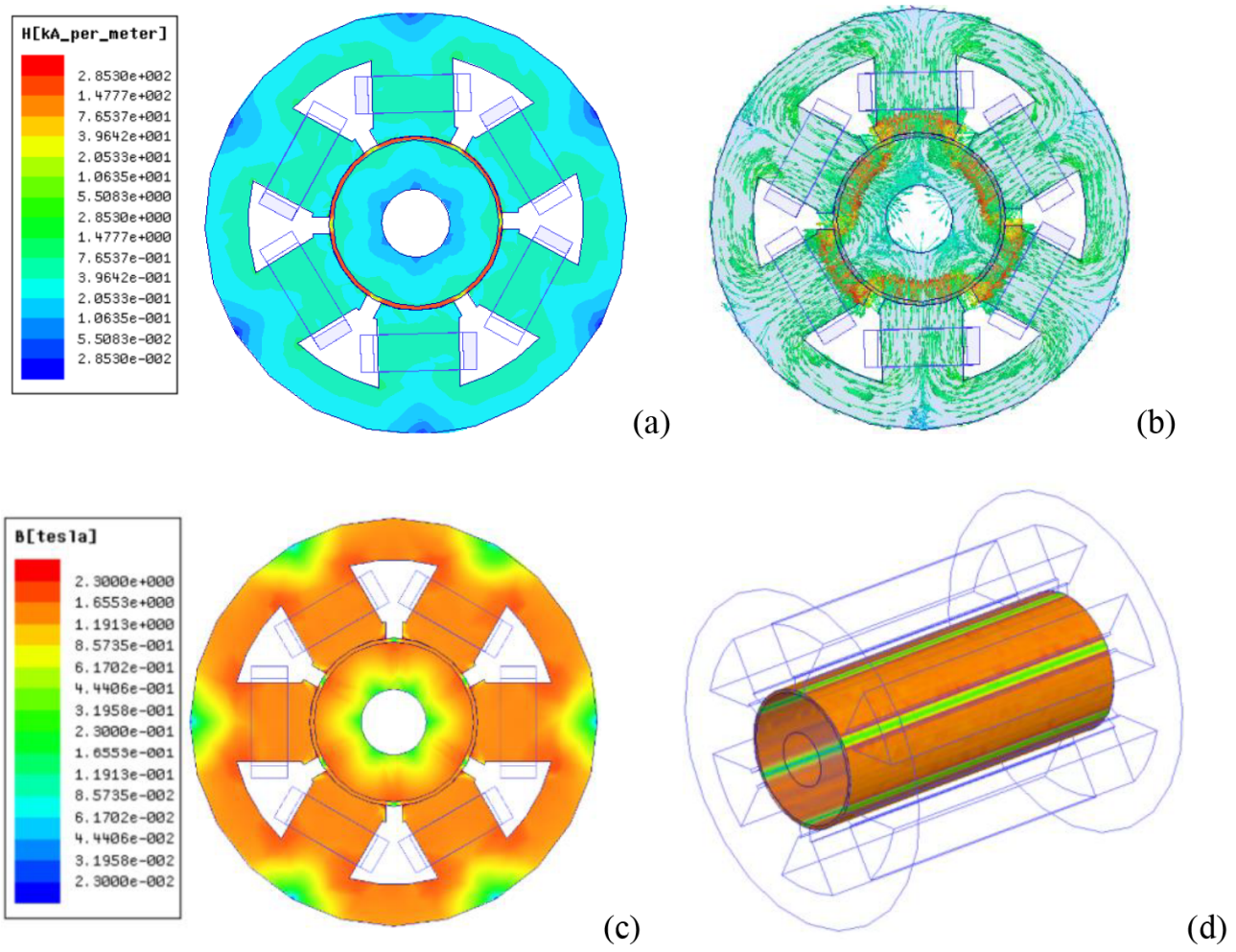

Figure 6. FEA results: (a) magnetic field strength, (b) magnetic flux flow direction, (c) magnetic induction in the MR brake cross-section, (d) magnetic induction distribution on the MR fluid along the length of the MR brake when the current is 1 A.

The MR brake's torque output was estimated by using Eq. (5) as 470 N with a current of 1 A. Moreover, the torque output of the design was calculated at various current levels and is shown in Figure 7. The torque response of the brake shows an almost linear relationship with the increased current.

3. Experiments and results

3.1. MR brake prototype and experimental setup

A prototype of the MR brake was manufactured to assess its performance. Coils were embedded to the stator and aluminum plates were placed tightly among the slots to prevent magnetic flux leakage between the pole heads. Figure 8 shows the manufactured brake and its stator structure with embedded coil wires. Silicone and

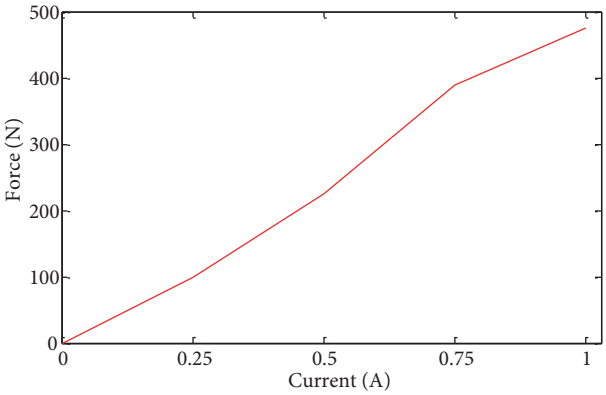

Figure 7. Torque–current relation from FEA results.

liquid gaskets were used to avoid any leakage from screw holes and linear ball bearings. The experimental setup is shown in Figure 9. A linear actuator was used to actuate the brake while the current input was regulated through an amplifier to generate braking forces. Output force was measured by a Zemic B3-D55 model load cell with capacity of 981 N (100 kg). The position of the MR brake rod was measured with a linear potentiometer. A Humusoft MF624 data acquisition card coupled with the MATLAB Real-Time Toolbox was used to control and collect the data in the experiments.

Figure 8. Manufactured MR brake prototype.

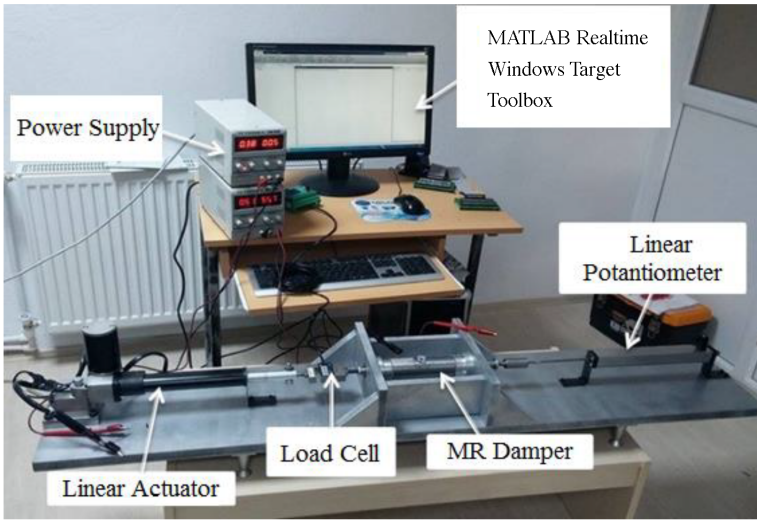

Figure 9. Experimental setup.

3.2. Experiments

3.2.1. Force response

The aim of this experiment was to determine the force response of the MR brake at different current levels. For this experiment, the linear actuator moved the MR brake piston at 5 mm/s while the current was varied from 0 A to 1 A. The force output at different currents is presented in Figure 10. The off-state force was measured at around 6 N, and the maximum force, where the current was set to 1 A, was measured as 480 N. The experimentally measured force is also very close to the force output from the FEA results (470 N). Moreover, hysteretic behavior was also observed when the current was lowered from 1 A to 0 A. In the experiments, the off-state force value was measured as 6 N before magnetization and it was about 15 N after the brake was activated. Due to the response time, Coulomb friction, viscous friction effects, hysteresis behavior, and modeling assumptions, there is a small difference between the simulation and the experimental force response in Figure 10.

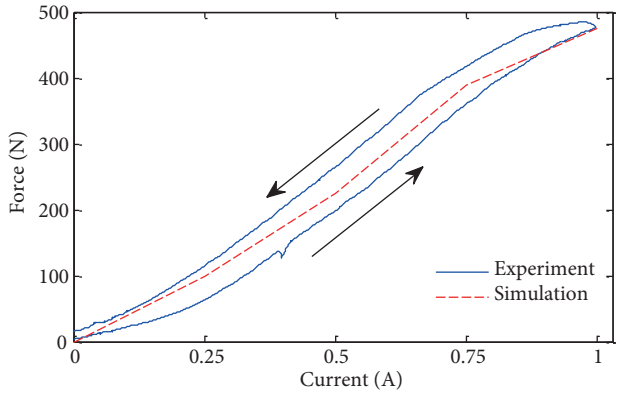

Figure 10. Force response of the linear MR brake at different current levels.

3.2.2. Transient force response

A set of experiments was conducted to determine the transient response characteristics and the time constant of the MR brake. The effect of the input current on the response was also investigated. The experiment was repeated for various current levels. The current was applied to the brake at these current levels after the rod had started to move, and the force output from the load cell was measured for 1 s. Figure 11 shows the transient force response for different currents. A first-order transfer function was fit to the response of the MR brake since the force output resembles a first-order system response. The time constant of the brake was determined as 40 ms. Similar behavior was observed for the different current levels.

3.2.3. Damping behavior

In this experiment, the MR brake was used to simulate a virtual damper. During the experiment, the force output was measured and the reference current values based on Eq. (10) were sent to the driver. In an ideal damper, output force should precisely follow the reference force calculated from Eq. (10):

$$F = bv, \tag{10}$$

where b and v are the damping coefficient and the velocity of the brake rod, respectively. For these experiments, we used a damping ratio of 20 Ns/mm. Figure 12 shows the damping experiment result of the brake.

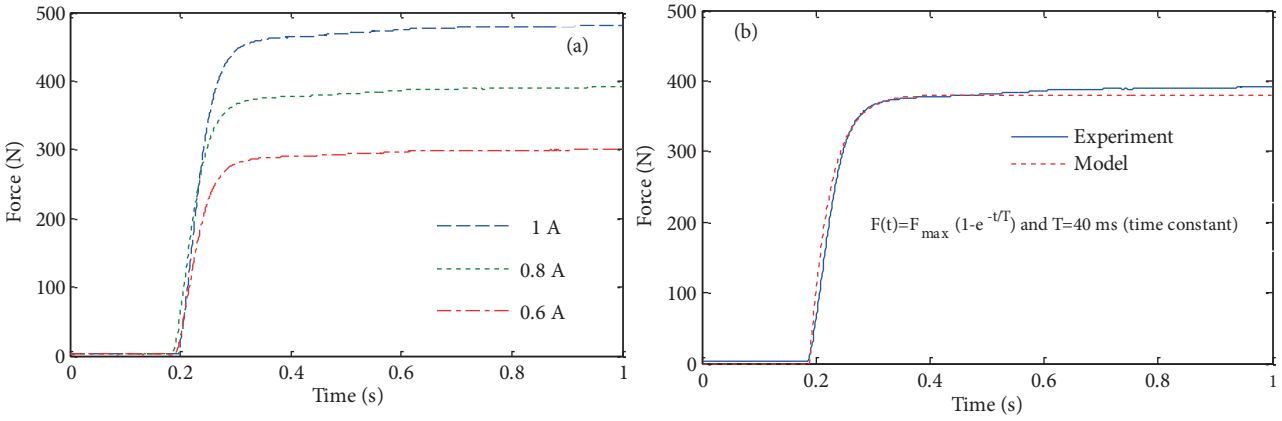

Figure 11. (a) Transient force response of the MR brake at different currents, (b) first-order transfer function fit for the transient response.

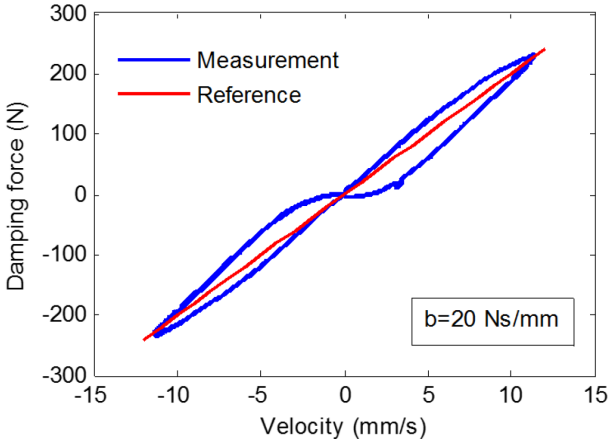

Figure 12. Damping experiment result.

4. Discussion

Our MR brake's force response, given in Figure 10, shows an almost linear relation with varying current. The force response of the brake also shows a hysteretic behavior due to the steel parts used in the brake design. The force output reaches 480 N around 1 A and its off-state friction force is very low (6 N) since the shear mode braking principle was used in the design. The proposed multipole outer coil linear MR brake design also needs to be compared with other linear brakes in the literature. To this end, the evaluation criteria proposed in [15] were used and Table 4 was created. These evaluation criteria are the cross-sectional area, stroke, maximum force, off-state force, ratio of maximum force to off-state force, required current at maximum force, and power consumption at maximum force. As the force output of the conventional piston cylinder type MR brake designs is independent from the brake length, it is not taken into consideration in the evaluation. Therefore, the brake cross-sectional area is more meaningful than the volume of the brake in the evaluation. The main objective of the proposed design in this study is to maximize on-state force while keeping the off-state force at very low levels; hence, the main evaluation criterion in Table 4 is the ratio of maximum force to off-state force. Our brake shows better performance than the others in terms of this criterion. Besides, the stroke of the proposed design can be increased as much as desired without increasing the brake length. Another advantage of the proposed design is that it requires a very low amount of MR fluid compared to the piston cylinder type MR brake designs.

On the other hand, the multipole outer coil linear MR brake requires a relatively large cross-sectional area due to its design complexity. Besides, the power consumption is high, since it requires a high amount of coil wire for the longitudinal multiple poles. Therefore, the proposed MR brake should be preferred in applications where power consumption is not critical.

Table 4. Comparison of MR brakes in the literature.

	Cross-sec area	Stroke (mm)	Max. force (N)	Off-state force (N)	Ratio of max. force to off-state force	Required current for max force (A)	Power consumption at max force (W)
Our MR brake	1963	∞	480	6	80	1	53
Alkan et al. [15]	712	∞	173	5.4	32	1	15
Shiao et al. [12]	2289	80	500	65	7.7	1.6	3.2
RD-8040-1 [24]	1392	55–74	2447	667	3.7	1	12
RD 1005 [5-7]	1134	50	451	52	8.7	1.5	18
SD 1000-2 [8]	1552	60	2100	270	7.8	1.5	-
Li et al. [9]	707	107	942	94	10	1	1.6
Milecki [10]	1963	50	15,000	4000	3.75	2.8	2.8
Gavin et al. [11]	1678	100	4000	300	13.3	10	60

5. Conclusion

This paper presented a new linear brake employing the shear mode braking principle with a multipole outer coil structure for high on-state and low off-state braking forces. The multipole outer stator design activates a large amount of MR fluid more efficiently by resetting the magnetic flux circuits in each pole. Thus, the MR fluid is activated more efficiently. To develop the design, analytical modeling, magnetic circuit analysis, design optimization, and magnetic FEA analysis of the design were introduced. Its manufacturing details and experimental results were also included. By the multipole outer coils structure, the proposed brake achieved high braking force (480 N) while keeping off-state force at a very low level (6 N). The ratio of the maximum force to off-state force of the multipole outer coils MR brake is 80, whereas it is a maximum of 32 in the best design in the literature. Additionally, it has infinite stroke and requires a low amount of MR fluid. The developed design is a good solution for some special applications such as haptics, stability in robotic devices, and steering stability in motorcycles, which require a wide range of variable braking forces from almost zero to high values. However, further minimizing the device size is the future work of this study.

Nomenclature

t_r	Rotor ring thickness	t_s	Stator ring thickness
R_r	Rotor radius	R_s	Stator radius
g	MR fluid gap	s	Slot thickness
c	Coil core thickness	z	Axial width
τ	Total shear stress	ν	Linear velocity
η	Viscosity of MR fluid	τ_y	Yield stress due to magnetic flux
F	Total braking force	$\dot{\gamma}$	Shear rate
F_{fr}	Force due to friction	F_{MR}	Force due to MR fluid magnetic field
N	Number of coil windings	F_{field}	Magnetic field force
R	Resistance	Φ	Magnetic flux

μ	Magnetic permeability	I	Electrical current
μ_{MR}	Magnetic permeability of MR fluid	μ_s	Magnetic permeability of steel
A	Area of a brake section	l	Length of a brake section
B	Magnetic flux density	H	Magnetic field strength
b	Damping coefficient	T	Time constant

Acknowledgment

The authors would like thank TÜBİTAK (The Scientific and Technological Research Council of Turkey) for the financial support of a research project numbered with TÜBİTAK-2209-A-1919B011401137. The authors declared that all authors contributed equally to this work.

References

[1] An J, Kwon DS. Haptic experimentation on a hybrid active/passive force feedback device. In: IEEE 2002 Robotics and Automation Conference; 11–15 May 2002; Washington, DC, USA. New York, NY, USA: IEEE. pp. 4217-4222.

[2] An J, Kwon DS. Five-bar linkage haptic device with DC motors and MR brakes. J Intell Mater Sys Struct 2008; 20: 1-12.

[3] Nam YJ, Park MK. A hybrid haptic device for wide-ranged force reflection and improved transparency. In: IEEE 2007 Control, Automation and Systems Conference; 17–20 October 2007; Seoul, Korea. New York, NY, USA: IEEE. pp. 1015-1020.

[4] Reed MR, Book WJ. Modeling and control of an improved dissipative passive haptic display. In: IEEE 2004 Robotics and Automation Conference; 26 April–1 May 2004; New Orleans, LA, USA. New York, NY, USA: IEEE pp. 311-318.

[5] Dominguez A, Sedaghati R, Stiharu I. A new dynamic hysteresis model for magnetorheological dampers. Smart Mater Struct 2006; 15: 1179-1189.

[6] Li WH, Yao GZ, Chen G, Yeo SH, Yap FF. Testing and steady state modeling of a linear MR damper under sinusoidal loading. Smart Mater Struct 2000; 9: 95-102.

[7] Xiang H, Fang Q, Gong Z, Wu H. Experimental investigation into magnetorheological damper subjected to impact loads. Transactions of Tianjin University 2008; 14: 540-544.

[8] Pang L, Kamath GM, Wereley NM. Analysis and testing of a linear magnetorheological damper. In: Proceedings of the 39th AIAA/ASME/ASCE/AHS/ASC Structures, Structural Dynamics, and Materials Conference and Exhibit and AIAA/ASME/AHS Adaptive Structures Forum; 20–23 April 1998; Long Beach, CA, USA. pp. 2841-2856.

[9] Li C, Furusho J, Morimoto S, Tokuda M, Hashimoto Y. Research and development of the intelligent prosthetic ankle joint with a MR linear brake. In: IEEE 2006 Electrorheological Fluids and Magnetorheological Suspensions Conference; 26–28 June 2006; Lake Tahoe, NV, USA. New York, NY, USA: IEEE. pp. 534-540.

[10] Milecki A. Investigation and control of magnetorheological fluid dampers. Int J Mach Tool Manu 2001; 41: 379-391.

[11] Gavin H, Hoagg J, Dobossy M. Optimal design of MR dampers. In: US–Japan 2001 Smart Structures for Improved Seismic Performance in Urban Regions Workshop; 14 August 2001; Seattle, WA, USA. pp. 225-236.

[12] Shiao Y, Kuo WH, Nguyen QH, Lai CW. Development of a variable damping magnetorheological damper with multiple poles. J Vibroeng 2015; 17: 1071-1078.

[13] Shiao Y, Chang CY. Design of an innovative high-torque brake. Adv Mat Res 2011; 339: 84-87.

[14] Shiao Y, Nguyen QA. Development of a multi-pole magnetorheological brake. Smart Mater Struct 2013; 22: 065008.

[15] Alkan SM, Gurocak H, Gonenc B. Linear magnetorheological brake with serpentine flux path as a high force and low off-state friction actuator for haptics. J Intell Mater Sys Struct 2013; 24: 1699-1713.

[16] Blake J, Gurocak H. Haptic glove with MR-brakes for virtual reality. IEEE ASME T Mech 2009; 14: 606-615.

[17] Xiaocong Z, Xinjiang J, Li C. Magnetorheological dampers: a review on structure design and analysis. J Intell Mater Sys Struct 2012; 28: 839-873.

[18] Lord Technical Data, MRF-140CG Magneto-Rheological Fluid, 2015.

[19] Lord Technical Data, MRF-132DG Magneto-Rheological Fluid, 2015.

[20] Lord Technical Data, MRF-122EG Magneto-Rheological Fluid, 2015.

[21] Ashour O, Rogers CA, Kordonsky W. Magnetorheological fluids: materials, characterization, and devices. J Intell Mater Sys Struct 2010; 7: 123-130.

[22] Nguyen QH, Choi SB. Optimal design of an automotive magnetorheological brake considering geometric dimensions and zero-field friction heat. Smart Mater Struct 2010; 19: 115024.

[23] Lord Corporation, Engineering Note, Magnetic Circuit Design, 1999.

[24] Lord Technical Data, RD-8040-1 MR Damper, 2015.